Fast and Accurate Solutions of Scattering Problems Involving Dielectric Objects with Moderate and Low Contrasts

Özgür Ergül[1,2] and Levent Gürel[1,2]

[1]*Department of Electrical and Electronics Engineering*
[2]*Computational Electromagnetics Research Center (BiLCEM)*
Bilkent University, TR-06800, Bilkent, Ankara, Turkey
ergul@ee.bilkent.edu.tr, lgurel@bilkent.edu.tr

***Abstract*— We consider the solution of electromagnetic scattering problems involving relatively large dielectric objects with moderate and low contrasts. Three-dimensional objects are discretized with Rao-Wilton-Glisson functions and the scattering problems are formulated with surface integral equations. The resulting dense matrix equations are solved iteratively by employing the multilevel fast multipole algorithm. We compare the accuracy and efficiency of the results obtained by employing various integral equations for the formulation of the problem. If the problem size is large, we show that a combined formulation, namely, electric-magnetic current combined-field integral equation, provides faster iterative convergence compared to other formulations, when it is accelerated with an efficient block preconditioner. For low-contrast problems, we introduce various stabilization procedures in order to avoid the numerical breakdown encountered in the conventional surface formulations.**

I. Introduction

Surface integral equations are commonly used to formulate scattering problems involving dielectric objects with arbitrary shapes [1]. By using equivalent electric and magnetic currents, boundary conditions are satisfied on the surface of the scatterer. In the literature, there are various integral-equation formulations derived by using different combinations of the boundary conditions and testing schemes [1]–[6]. When the problem size is large, discretizations of the integral-equation formulations lead to large matrix equations, which can be solved iteratively with accelerated matrix-vector multiplications by the multilevel fast multipole algorithm (MLFMA) [7]. On the other hand, efficient solutions require rapid convergence of the iterations, which depends on the formulation. In addition, accuracy of the results also depends on the formulation type, even if the formulations are discretized in the same way. In this paper, we extensively compare various surface formulations in terms of efficiency and accuracy. Specifically, we consider the combined T formulation (CTF), the modified N-Müller formulation (MNMF), and the electric-magnetic current combined-field integral equation (JMCFIE), which are developed recently for stable solutions of dielectric problems. These formulations are compared by solving scattering problems involving dielectric spheres of various sizes discretized with 4000 to 3,000,000 unknowns.

When the contrast of the object is low, i.e., when the electric properties of the inner and outer media are close the each other, conventional surface formulations become inaccurate to calculate the scattered fields. For accurate solutions, conventional formulations should be stabilized by extracting the nonradiating currents and solving the equations only for the radiating currents. In this paper, we introduce various stabilization procedures involving different arrangements of the right-hand sides (RHSs) of the equations. Using a novel field-based stabilization technique, we obtain accurate results for arbitrarily low-contrast problems, even when the contrast of the object is extremely low. The stabilization procedures are presented for CTF, while they are also applicable to other conventional formulations.

II. Surface Formulations of Dielectric Problems

In the surface formulations of scattering problems involving homogenous dielectric objects, the operators are defined as

$$\mathcal{T}_l\{\boldsymbol{X}(\boldsymbol{r})\} = ik_l \int_S d\boldsymbol{r'}\Big[\boldsymbol{X}(\boldsymbol{r'}) + \frac{1}{k_l^2}\nabla\nabla'\cdot\boldsymbol{X}(\boldsymbol{r'})\Big] g_l(\boldsymbol{r},\boldsymbol{r'}) \tag{1}$$

$$\mathcal{K}_l\{\boldsymbol{X}(\boldsymbol{r})\} = \int_{PV,S} d\boldsymbol{r'}\boldsymbol{X}(\boldsymbol{r'})\times\nabla' g_l(\boldsymbol{r},\boldsymbol{r'}) \tag{2}$$

$$\mathcal{I}\{\boldsymbol{X}(\boldsymbol{r})\} = \boldsymbol{X}(\boldsymbol{r}) \tag{3}$$

for outside ($l=1$) and inside ($l=2$) the object. In (1) and (2), S is the surface of the object, PV indicates the principal value of the integral, $k_l = w\sqrt{\mu_l\epsilon_l}$ is the wavenumber associated with medium l, and

$$g_l(\boldsymbol{r},\boldsymbol{r'}) = \frac{\exp(ik_lR)}{4\pi R} \qquad \Big(R = |\boldsymbol{r}-\boldsymbol{r'}|\Big) \tag{4}$$

is the homogenous-space Green's function. Using the operators in (1)-(3), scattered electric and magnetic fields can be obtained from the surface equivalent currents, i.e.,

$$\boldsymbol{J}(\boldsymbol{r}) = \hat{\boldsymbol{n}}\times\boldsymbol{H}(\boldsymbol{r}) \tag{5}$$

$$\boldsymbol{M}(\boldsymbol{r}) = -\hat{\boldsymbol{n}}\times\boldsymbol{E}(\boldsymbol{r}). \tag{6}$$

Then, the boundary conditions for the tangential fields are enforced on the surface of the scatterer to calculate the unknown equivalent currents, as well as the scattered electric and magnetic fields. In the literature, there are various integral-equation formulations derived by using different combinations of the boundary conditions and testing schemes [1]–[6]. For example, the T formulations are obtained when the boundary conditions are tested directly by using the tangential unit vector $\hat{\boldsymbol{t}}$ at the observation point. Among various T formulations, CTF is derived as [5]

$$\hat{\boldsymbol{t}}\cdot\begin{bmatrix} \mathcal{Z}_{11}^T & \mathcal{Z}_{12}^T \\ \mathcal{Z}_{21}^T & \mathcal{Z}_{22}^T \end{bmatrix}\cdot\begin{bmatrix} \boldsymbol{J}(\boldsymbol{r}) \\ \boldsymbol{M}(\boldsymbol{r}) \end{bmatrix} = -\hat{\boldsymbol{t}}\cdot\begin{bmatrix} \eta_1^{-1}\boldsymbol{E}^{inc}(\boldsymbol{r}) \\ \eta_1\boldsymbol{H}^{inc}(\boldsymbol{r}) \end{bmatrix}, \tag{7}$$

where

$$\mathcal{Z}_{11}^T = \mathcal{Z}_{22}^T = \mathcal{T}_1 + \mathcal{T}_2 \tag{8}$$
$$\mathcal{Z}_{12}^T = -\eta_1^{-1}\mathcal{K}_1 - \eta_2^{-1}\mathcal{K}_2 + 0.5\big(\eta_2^{-1} - \eta_1^{-1}\big)\hat{\boldsymbol{n}}\times\mathcal{I} \tag{9}$$
$$\mathcal{Z}_{21}^T = \eta_1\mathcal{K}_1 + \eta_2\mathcal{K}_2 + 0.5\big(\eta_1 - \eta_2\big)\hat{\boldsymbol{n}}\times\mathcal{I}. \tag{10}$$

In (7)–(10), $\boldsymbol{E}^{inc}(\boldsymbol{r})$ and $\boldsymbol{H}^{inc}(\boldsymbol{r})$ are the incident electric and magnetic fields, $\eta_l = \sqrt{\mu_l/\epsilon_l}$ is the impedance of the medium $l = 1, 2$, and $\hat{\boldsymbol{n}}$ is the outward normal vector on the surface.

In contrast to the T formulations, N formulations involve a projection operation using the unit normal vector $\hat{\boldsymbol{n}}$. For example, MNMF can be derived as [4]

$$\hat{\boldsymbol{n}}\times\begin{bmatrix} \mathcal{Z}_{11}^N & \mathcal{Z}_{12}^N \\ \mathcal{Z}_{21}^N & \mathcal{Z}_{22}^N \end{bmatrix}\cdot\begin{bmatrix} \boldsymbol{J}(\boldsymbol{r}) \\ \boldsymbol{M}(\boldsymbol{r}) \end{bmatrix} = -\hat{\boldsymbol{n}}\times\begin{bmatrix} \mu_1\boldsymbol{H}^{inc}(\boldsymbol{r})/(\mu_1+\mu_2) \\ -\epsilon_1\boldsymbol{E}^{inc}(\boldsymbol{r})/(\epsilon_1+\epsilon_2) \end{bmatrix}, \tag{11}$$

where

$$\mathcal{Z}_{11}^N = \frac{\mu_1}{\mu_1+\mu_2}\mathcal{K}_1 - \frac{\mu_2}{\mu_1+\mu_2}\mathcal{K}_2 + 0.5\hat{\boldsymbol{n}}\times\mathcal{I} \tag{12}$$
$$\mathcal{Z}_{12}^N = \frac{\mu_1}{\mu_1+\mu_2}\eta_1^{-1}\mathcal{T}_1 - \frac{\mu_2}{\mu_1+\mu_2}\eta_2^{-1}\mathcal{T}_2 \tag{13}$$
$$\mathcal{Z}_{21}^N = -\frac{\epsilon_1}{\epsilon_1+\epsilon_2}\eta_1\mathcal{T}_1 + \frac{\epsilon_2}{\epsilon_2+\epsilon_2}\eta_2\mathcal{T}_2 \tag{14}$$
$$\mathcal{Z}_{22}^N = \frac{\epsilon_1}{\epsilon_1+\epsilon_2}\mathcal{K}_1 - \frac{\epsilon_2}{\epsilon_1+\epsilon_2}\mathcal{K}_2 + 0.5\hat{\boldsymbol{n}}\times\mathcal{I}. \tag{15}$$

Both CTF and MNMF are free of the internal-resonance problem and provide stable solutions.

In this paper, we investigate the efficiency and accuracy of the T and N formulations when they are discretized with Rao-Wilton-Glisson (RWG) functions defined on planar triangles. Adopting a Galerkin scheme, we use the same set of RWG functions as the basis and testing functions. In general, the T and N formulations are similar to the electric-field integral equation (EFIE) and the magnetic-field integral equation (MFIE), respectively, for perfectly-conducting objects. We also consider the counterpart of the combined-field integral equation (CFIE), namely, JMCFIE [6], derived as

$$\begin{bmatrix} \mathcal{Z}_{11}^{TN} & \mathcal{Z}_{12}^{TN} \\ \mathcal{Z}_{21}^{TN} & \mathcal{Z}_{22}^{TN} \end{bmatrix}\cdot\begin{bmatrix} \boldsymbol{J}(\boldsymbol{r}) \\ \boldsymbol{M}(\boldsymbol{r}) \end{bmatrix} = -\begin{bmatrix} v_a^{TN} \\ v_b^{TN} \end{bmatrix}, \tag{16}$$

where

$$\mathcal{Z}_{11}^{TN} = \mathcal{Z}_{22}^{TN} = \hat{\boldsymbol{t}}\cdot(\mathcal{T}_1+\mathcal{T}_2) + \hat{\boldsymbol{n}}\times(\mathcal{K}_1-\mathcal{K}_2) - \mathcal{I} \tag{17}$$
$$\mathcal{Z}_{12}^{TN} = \hat{\boldsymbol{t}}\cdot(-\eta_1^{-1}\mathcal{K}_1 - \eta_2^{-1}\mathcal{K}_2) + \hat{\boldsymbol{n}}\times(\eta_1^{-1}\mathcal{T}_1 - \eta_2^{-1}\mathcal{T}_2) + 0.5\big(\eta_2^{-1}-\eta_1^{-1}\big)\hat{\boldsymbol{t}}\cdot\hat{\boldsymbol{n}}\times\mathcal{I} \tag{18}$$
$$\mathcal{Z}_{21}^{TN} = \hat{\boldsymbol{t}}\cdot(\eta_1\mathcal{K}_1 + \eta_2\mathcal{K}_2) + \hat{\boldsymbol{n}}\times(-\eta_1\mathcal{T}_1 + \eta_2\mathcal{T}_2) + 0.5\big(\eta_1-\eta_2\big)\hat{\boldsymbol{t}}\cdot\hat{\boldsymbol{n}}\times\mathcal{I} \tag{19}$$

and

$$v_a^{TN} = \eta_1^{-1}\hat{\boldsymbol{t}}\cdot\boldsymbol{E}^{inc}(\boldsymbol{r}) + \hat{\boldsymbol{n}}\times\boldsymbol{H}^{inc}(\boldsymbol{r}) \tag{20}$$
$$v_b^{TN} = \eta_1\hat{\boldsymbol{t}}\cdot\boldsymbol{H}^{inc}(\boldsymbol{r}) - \hat{\boldsymbol{n}}\times\boldsymbol{E}^{inc}(\boldsymbol{r}). \tag{21}$$

Similar to CFIE, JMCFIE produces well-conditioned matrix equations, which are crucial for iterative solutions.

III. Iterative Solutions of Surface Formulations by MLFMA

For the simultaneous discretization of the integral equations and the scatterer surface, unknown current densities are expanded in a series of basis functions, i.e.,

$$\boldsymbol{J}(\boldsymbol{r}) = \hat{\boldsymbol{n}}\times\boldsymbol{H}(\boldsymbol{r}) = \sum_{n=1}^{N} x_n\boldsymbol{b}_n(\boldsymbol{r}) \tag{22}$$
$$\boldsymbol{M}(\boldsymbol{r}) = -\hat{\boldsymbol{n}}\times\boldsymbol{E}(\boldsymbol{r}) = \sum_{n=1}^{N} y_n\boldsymbol{b}_n(\boldsymbol{r}). \tag{23}$$

Testing the integral equations on the surface, $2N\times 2N$ matrix equations are constructed as

$$\begin{bmatrix} \bar{\boldsymbol{Z}}_{11} & \bar{\boldsymbol{Z}}_{12} \\ \bar{\boldsymbol{Z}}_{21} & \bar{\boldsymbol{Z}}_{22} \end{bmatrix}\cdot\begin{bmatrix} \boldsymbol{x} \\ \boldsymbol{y} \end{bmatrix} = \begin{bmatrix} \boldsymbol{v}_1^{inc} \\ \boldsymbol{v}_2^{inc} \end{bmatrix}, \tag{24}$$

where the matrix elements correspond to the interactions of the basis and testing functions and the RHS vector is obtained by testing the incident fields. We note that the matrix elements involve combinations of discretized operators depending on the formulation. Considering the nth basis function $\boldsymbol{b}_n(\boldsymbol{r})$ and the mth testing function $\boldsymbol{t}_m(\boldsymbol{r})$, $\mathcal{K}$ and $\mathcal{T}$ operators are discretized as

$$\hat{\boldsymbol{t}}\cdot\mathcal{K} \to \overline{\boldsymbol{K}}_l^T[m,n] = \Big\langle \boldsymbol{t}_m(\boldsymbol{r}), \mathcal{K}_l\{\boldsymbol{b}_n(\boldsymbol{r})\}\Big\rangle \tag{25}$$
$$\hat{\boldsymbol{n}}\times\mathcal{K} \to \overline{\boldsymbol{K}}_l^N[m,n] = \Big\langle \boldsymbol{t}_m(\boldsymbol{r}), \hat{\boldsymbol{n}}\times\mathcal{K}_l\{\boldsymbol{b}_n(\boldsymbol{r})\}\Big\rangle \tag{26}$$
$$\hat{\boldsymbol{t}}\cdot\mathcal{T} \to \overline{\boldsymbol{T}}_l^T[m,n] = \Big\langle \boldsymbol{t}_m(\boldsymbol{r}), \mathcal{T}_l\{\boldsymbol{b}_n(\boldsymbol{r})\}\Big\rangle \tag{27}$$
$$\hat{\boldsymbol{n}}\times\mathcal{T} \to \overline{\boldsymbol{T}}_l^N[m,n] = \Big\langle \boldsymbol{t}_m(\boldsymbol{r}), \hat{\boldsymbol{n}}\times\mathcal{T}_l\{\boldsymbol{b}_n(\boldsymbol{r})\}\Big\rangle \tag{28}$$

where

$$\Big\langle \boldsymbol{t}_m(\boldsymbol{r}), \boldsymbol{f}(\boldsymbol{r})\Big\rangle = \int_{S_m} d\boldsymbol{r}\boldsymbol{t}_m(\boldsymbol{r})\cdot\boldsymbol{f}(\boldsymbol{r}) \tag{29}$$

is an integral on the support of the testing function S_m.

The matrix equation in (24) can be solved iteratively, where the matrix-vector multiplications are performed efficiently with MLFMA [7]. In MLFMA, only the near-field interactions are computed directly by calculating the integrals

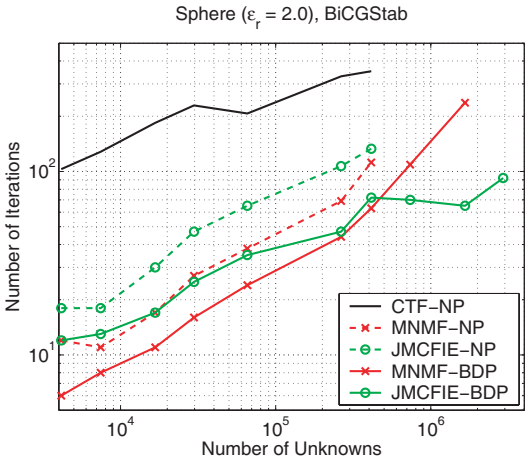

Fig. 1. Number of BiCGStab iterations (10^{-3} residual error) for the solution of scattering problems involving spheres of various radii from $0.75\lambda_1$ to $20\lambda_1$ discretized with $\lambda_1/10$ mesh size.

on the basis and testing domains. On the other hand, far-field interactions are calculated approximately in a group-by-group manner using the factorization and diagonalization of the Green's function. First, the scatterer is included in a cubic box and the computational domain is recursively divided into subboxes (clusters). Then, a multilevel tree structure is constructed by considering the nonempty clusters in all levels. MLFMA involves three main stages performed on the tree structure.

1) Aggregation: Radiated fields at the centers of the clusters are calculated from the bottom of the tree structure to the highest level.
2) Translation: Radiated fields at the centers of the clusters are translated into incoming fields for other clusters.
3) Disaggregation: The total incoming fields at the centers of the clusters are calculated from the top of the tree structure to the lowest level. At the lowest level, the incoming fields are received by the testing functions.

In the solution of dielectric problems with moderate and low contrasts, we employ the same tree structure for both the inner and the outer media. However, the sampling rate for the radiated and incoming fields as well as the number of harmonics for the translation operators depend on the wavenumber. Therefore, an accurate calculation of the interactions requires two separate versions of MLFMA to perform the matrix-vector multiplications related to the inner and outer media. Using MLFMA, matrix-vector multiplications can be performed in $O(N \log N)$ time using $O(N \log N)$ memory. The details of MLFMA can be found in [3],[7].

IV. Accuracy and Efficiency of the Solutions

Using a Galerkin scheme, N formulations, such as MNMF in (11), contain well-tested identity operators, i.e.,

$$\left\langle \boldsymbol{t}_m(\boldsymbol{r}), \boldsymbol{b}_n(\boldsymbol{r}) \right\rangle = \int_{S_m} d\boldsymbol{r} \boldsymbol{t}_m(\boldsymbol{r}) \cdot \boldsymbol{b}_n(\boldsymbol{r}) \tag{30}$$

These strong interactions are located on the diagonal blocks of the matrix equations. On the other hand, T formulations, such as CTF in (7), contain weakly-tested identity operators, i.e.,

$$\left\langle \boldsymbol{t}_m(\boldsymbol{r}), \hat{\boldsymbol{n}} \times \boldsymbol{b}_n(\boldsymbol{r}) \right\rangle = \int_{S_m} d\boldsymbol{r} \boldsymbol{t}_m(\boldsymbol{r}) \cdot \hat{\boldsymbol{n}} \times \boldsymbol{b}_n(\boldsymbol{r}) \tag{31}$$

that are located on the non-diagonal blocks. For some T formulations, the identity operators may completely vanish. Since the T and N formulations have different forms of identity operators, the two types of formulations show different behaviors in terms of accuracy and conditioning.

1) N formulations are usually better conditioned than the T formulations [5],[8]. Therefore, iterative solutions of the N formulations are easier and they can be further accelerated by employing simple and efficient preconditioners.
2) Although they are better conditioned, N formulations can be considerably less accurate compared to the T formulations for the same discretization [5],[9]. The source of the error is the identity operators and it becomes evident when the discretization is performed with the low-order RWG functions.

To compare the dielectric formulations in terms of efficiency, Fig. 1 demonstrates the solutions of scattering problems involving spheres of various radii from $0.75\lambda_1$ to $20\lambda_1$, where λ_1 is the wavelength in the outer medium. The relative permittivity (ϵ_r) of the inner medium is 2.0. Discretizations with $\lambda_1/10$ mesh size produce matrix equations with numbers of unknowns from 4142 to 2,925,708. Spheres are illuminated by a plane wave propagating in the z direction with the electric field polarized in the x direction. Each problem is formulated by CTF, MNMF, and JMCFIE, and the resulting matrix equations are solved iteratively using MLFMA. Both near-field and far-field interactions are computed with 1% error. As the iterative solver, we employ the biconjugate-gradient-stabilized (BiCGStab) algorithm. In addition, we use a block preconditioner (BP) to accelerate the solutions of MNMF and JMCFIE by transforming the original matrix equation as

$$\bar{\boldsymbol{P}}^{-1} \cdot \begin{bmatrix} \bar{\boldsymbol{Z}}_{11} & \bar{\boldsymbol{Z}}_{12} \\ \bar{\boldsymbol{Z}}_{21} & \bar{\boldsymbol{Z}}_{22} \end{bmatrix} \cdot \begin{bmatrix} \boldsymbol{x} \\ \boldsymbol{y} \end{bmatrix} = \bar{\boldsymbol{P}}^{-1} \cdot \begin{bmatrix} \boldsymbol{v}_1^{inc} \\ \boldsymbol{v}_2^{inc} \end{bmatrix}, \tag{32}$$

where $\bar{\boldsymbol{P}}$ is the preconditioner matrix. To construct BP, we consider the self interactions of the lowest level clusters, i.e.,

$$\bar{\boldsymbol{P}} = \begin{bmatrix} \bar{\boldsymbol{P}}_{11} & \bar{\boldsymbol{P}}_{12} \\ \bar{\boldsymbol{P}}_{21} & \bar{\boldsymbol{P}}_{22} \end{bmatrix}, \tag{33}$$

where $\bar{\boldsymbol{P}}_{ab}$ are block-diagonal matrices. Then, the inverse of $\bar{\boldsymbol{P}}$ can be evaluated efficiently as [10]

$$\bar{\boldsymbol{P}}^{-1} = \begin{bmatrix} \bar{\boldsymbol{B}}_{11} & \bar{\boldsymbol{B}}_{12} \\ \bar{\boldsymbol{B}}_{21} & \bar{\boldsymbol{B}}_{22} \end{bmatrix}, \tag{34}$$

where

$$\bar{\boldsymbol{B}}_{11} = \bar{\boldsymbol{P}}_{11}^{-1} \left[\bar{\boldsymbol{I}} + \bar{\boldsymbol{P}}_{12} \cdot \bar{\boldsymbol{S}}^{-1} \cdot \bar{\boldsymbol{P}}_{21} \cdot \bar{\boldsymbol{P}}_{11}^{-1} \right] \tag{35}$$

$$\bar{\boldsymbol{B}}_{12} = -\bar{\boldsymbol{P}}_{11}^{-1} \cdot \bar{\boldsymbol{P}}_{12} \cdot \bar{\boldsymbol{S}}^{-1} \tag{36}$$

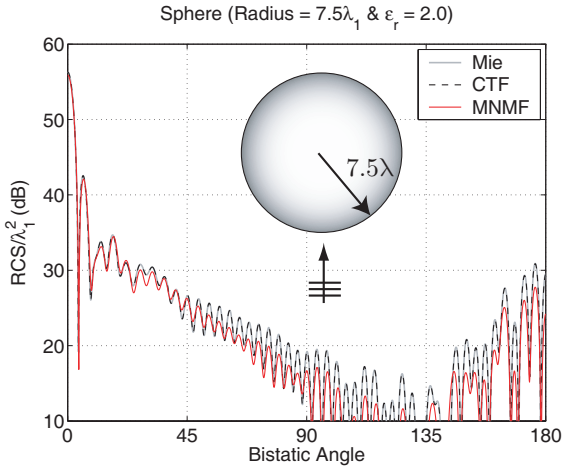

(a)

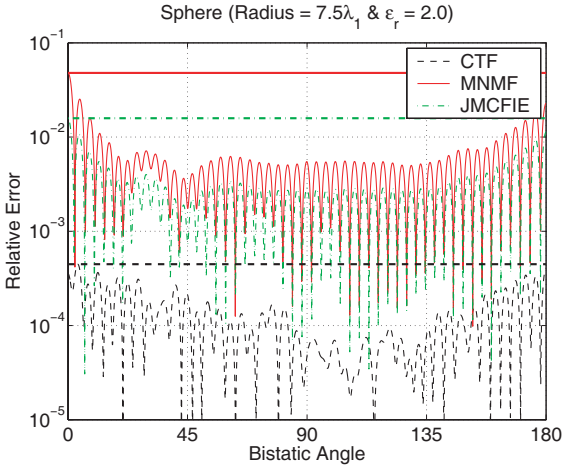

(b)

Fig. 2. (a) Normalized bistatic RCS (RCS/λ_1^2) of a sphere of radius $7.5\lambda_1$ with a relative permittivity of 2.0 in free space. (b) Relative error defined in (39) for different formulations as a function of the bistatic angle.

$$\bar{\boldsymbol{B}}_{21} = -\bar{\boldsymbol{S}}^{-1} \cdot \bar{\boldsymbol{P}}_{21} \cdot \bar{\boldsymbol{P}}_{11}^{-1} \tag{37}$$

$$\bar{\boldsymbol{B}}_{22} = \bar{\boldsymbol{S}}^{-1} \tag{38}$$

and $\bar{\boldsymbol{S}} = \bar{\boldsymbol{P}}_{22} - \bar{\boldsymbol{P}}_{21} \cdot \bar{\boldsymbol{P}}_{11}^{-1} \cdot \bar{\boldsymbol{P}}_{12}$ is the Schur complement of $\bar{\boldsymbol{P}}_{11}$. In Fig. 1, we present the iteration counts to reduce the residual error below 0.001. Without preconditioning, MNMF offers faster convergence compared to JMCFIE and CTF, while CTF has the slowest convergence. Using BP, convergence of MNMF and JMCFIE can be accelerated further, while the convergence of CTF becomes worse when BP is applied (not shown in the figure). For large problems, BP reduces the iteration counts for JMCFIE so effectively that JMCFIE converges faster than MNMF. As the problem size gets larger, the processing time for the setup of MLFMA, including the calculation of the near-field interactions, radiation and receiving patterns of the basis and testing functions, and translation operators, becomes negligible compared to the time required for the iterative solution. Consequently, for the solution of large problems, JMCFIE becomes the most efficient formulation (even though its setup time is usually longer than the time required for CTF and MNMF) when it is accelerated with BP.

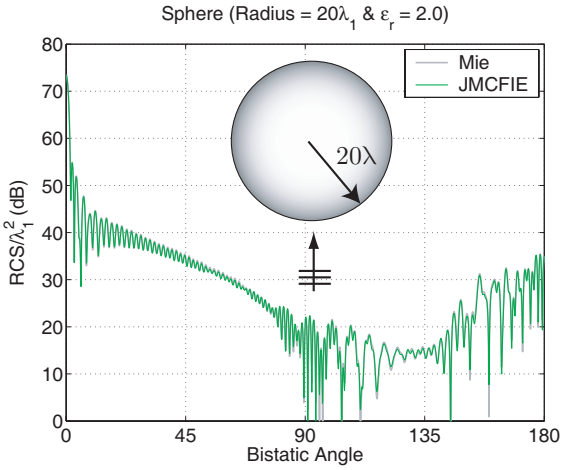

Fig. 3. Normalized bistatic RCS (RCS/λ_1^2) of a sphere of radius $20\lambda_1$ with a relative permittivity of 2.0 in free space.

Fig. 2(a) presents the normalized bistatic radar cross section (RCS/λ_1^2) values in decibels (dB) for a sphere of radius $7.5\lambda_1$ and $\epsilon_r = 2.0$. Analytical values obtained by a Mie-series solution are plotted as a reference from 0° to 180°, where 0° corresponds to the forward-scattering direction. Fig. 2(a) shows that the computational values obtained with CTF are close to the analytical results and they are more accurate compared to the results of MNMF. For a more quantitative comparison, Fig. 2(b) presents a relative error defined as

$$e(\theta) = \frac{|E_a(\theta) - E_c(\theta)|}{\max_\theta |E_a(\theta)|} \tag{39}$$

with respect to bistatic angle θ, where $E_a(\theta)$ and $E_c(\theta)$ are analytical and computation values, respectively, for the co-polar electric field. In addition to CTF and MNMF, we also consider the relative error for JMCFIE. The maximum value of the relative error for each formulation is also indicated in the plot. We observe that CTF is the most accurate formulation, while JMCFIE is more accurate than MNMF. In general, the choice of the formulation depends on the application. CTF offers more accurate results with low efficiency, while JMCFIE becomes preferable for faster solutions.

Finally, Fig. 3 presents the bistatic RCS values for a sphere of radius 20λ and $\epsilon_r = 2.0$ discretized with 2,925,708 unknowns. The computational values obtained with JMCFIE are close to the analytical curve obtained by a Mie-series solution. The maximum relative error is 2.4%. This problem cannot be solved in a reasonable number of iterations when it is formulated with CTF or MNMF.

V. Low-Contrast Breakdown and Stabilization of Surface Formulations

Conventional surface formulations, such as CTF, MNMF, and JMCFIE, are stable and provide accurate results when they are used to formulate problems involving moderate values

of dielectric parameters. However, these formulations tend to be less accurate as the contrast of the object decreases and the electromagnetic material properties of the inner and outer media converge to each other. There are various applications that involve scattering from low-contrast objects. Examples are plastic mines buried in soil [11], polymeric materials, such as sub-micron latex particles in water [12], red blood cells in blood plasma [13], and dielectric photonic crystals [14]. When the contrast is low, however, it becomes difficult to obtain accurate results with the conventional surface formulations unless a stabilization procedure is applied.

Low-contrast breakdown of the surface formulations is due to relatively large nonradiating parts of the induced currents on the scatterer [15]. For any arbitrary solution, equivalent electric and magnetic currents on the surface of the object can be decomposed as

$$\begin{aligned}\boldsymbol{J}(\boldsymbol{r}) &= \hat{\boldsymbol{n}} \times \boldsymbol{H}(\boldsymbol{r}) = \hat{\boldsymbol{n}} \times \boldsymbol{H}^{inc}(\boldsymbol{r}) + \hat{\boldsymbol{n}} \times \boldsymbol{H}^{r}(\boldsymbol{r}) \\ &= \boldsymbol{J}^{inc}(\boldsymbol{r}) + \boldsymbol{J}^{r}(\boldsymbol{r}) \qquad (40)\\ \boldsymbol{M}(\boldsymbol{r}) &= -\hat{\boldsymbol{n}} \times \boldsymbol{E}(\boldsymbol{r}) = -\hat{\boldsymbol{n}} \times \boldsymbol{E}^{inc}(\boldsymbol{r}) - \hat{\boldsymbol{n}} \times \boldsymbol{E}^{r}(\boldsymbol{r}) \\ &= \boldsymbol{M}^{inc}(\boldsymbol{r}) + \boldsymbol{M}^{r}(\boldsymbol{r}), \qquad (41)\end{aligned}$$

where $\{\boldsymbol{J}^{inc}(\boldsymbol{r}), \boldsymbol{M}^{inc}(\boldsymbol{r})\} = \{\hat{\boldsymbol{n}} \times \boldsymbol{H}^{inc}(\boldsymbol{r}), -\hat{\boldsymbol{n}} \times \boldsymbol{E}^{inc}(\boldsymbol{r})\}$ do not radiate. When the contrast of the object is small, these nonradiating currents dominate the total currents. Then, it becomes difficult to perform the calculations accurately enough to capture the small radiating currents properly. In other words, even though the surface currents $\boldsymbol{J}(\boldsymbol{r})$ and $\boldsymbol{M}(\boldsymbol{r})$ are computed with relatively small error, scattered fields cannot be obtained accurately from them.

For accurate solutions of low-contrast dielectric problems, the conventional formulations can be modified by extracting the incident fields from the total currents and solving only the radiating currents as the unknowns of the problem [15]. To apply this stabilization procedure, we consider a modified version of CTF derived as

$$\hat{\boldsymbol{t}} \cdot \begin{bmatrix} \eta_1\mathcal{T}_1 + \eta_2\mathcal{T}_2 & -\left(\mathcal{K}_1 + \mathcal{K}_2\right) \\ \eta_1\eta_2\left(\mathcal{K}_1 + \mathcal{K}_2\right) & \eta_2\mathcal{T}_1 + \eta_1\mathcal{T}_2 \end{bmatrix} \cdot \begin{bmatrix} \boldsymbol{J}(\boldsymbol{r}) \\ \boldsymbol{M}(\boldsymbol{r}) \end{bmatrix} = -\hat{\boldsymbol{t}} \cdot \begin{bmatrix} \boldsymbol{E}^{inc}(\boldsymbol{r}) \\ \eta_2\eta_1\boldsymbol{H}^{inc}(\boldsymbol{r}) \end{bmatrix}. \qquad (42)$$

Extracting the nonradiating currents and rearranging the equation, we obtain the stable CTF (S-CTF) as [16]

$$\hat{\boldsymbol{t}} \cdot \begin{bmatrix} \eta_1\mathcal{T}_1 + \eta_2\mathcal{T}_2 & -\left(\mathcal{K}_1 + \mathcal{K}_2\right) \\ \eta_1\eta_2\left(\mathcal{K}_1 + \mathcal{K}_2\right) & \eta_2\mathcal{T}_1 + \eta_1\mathcal{T}_2 \end{bmatrix} \cdot \begin{bmatrix} \boldsymbol{J}^{r}(\boldsymbol{r}) \\ \boldsymbol{M}^{r}(\boldsymbol{r}) \end{bmatrix} = \hat{\boldsymbol{t}} \cdot \begin{bmatrix} \eta_1\mathcal{T}_1 - \eta_2\mathcal{T}_2 & -\left(\mathcal{K}_1 - \mathcal{K}_2\right) \\ \eta_1\eta_2\left(\mathcal{K}_1 - \mathcal{K}_2\right) & \eta_2\mathcal{T}_1 - \eta_1\mathcal{T}_2 \end{bmatrix} \cdot \begin{bmatrix} \boldsymbol{J}^{inc}(\boldsymbol{r}) \\ \boldsymbol{M}^{inc}(\boldsymbol{r}) \end{bmatrix}. \qquad (43)$$

We note that the left-hand side (LHS) of the stable formulation is the same as the LHS of CTF. In other words, the stabilization procedure requires a modification only on the RHS of the conventional formulation.

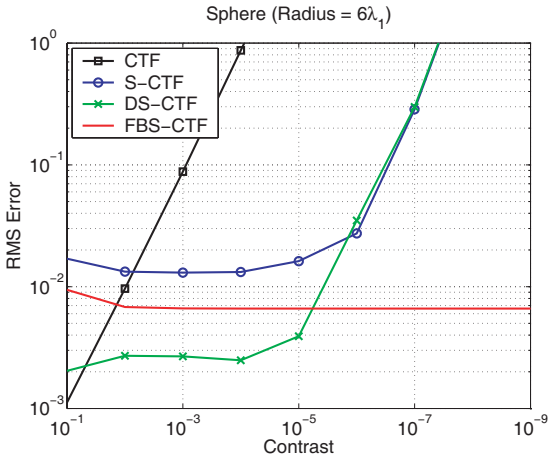

(a)

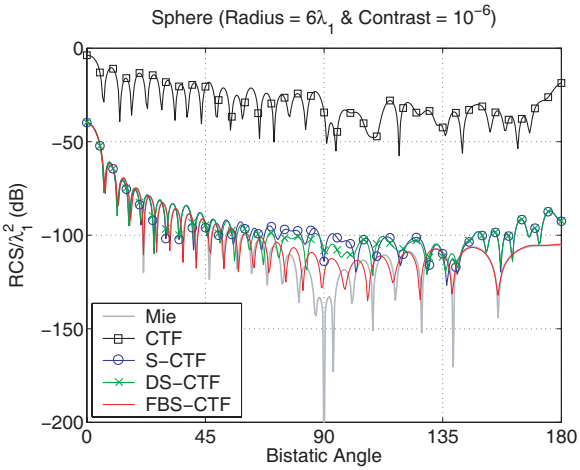

(b)

Fig. 4. (a) Relative RMS error defined in (47) for the solutions of the scattering problems involving a sphere of radius $6\lambda_1$ with different contrasts. (b) Normalized bistatic RCS (RCS/λ_1^2) of a sphere of radius $6\lambda_1$ and permittivity $1 + 10^{-6}$ in free space.

On the RHS, S-CTF involves operators applied on the incident fields, which can be evaluated directly by expanding the fields in a series of basis functions and performing matrix-vector multiplications [17]. The expansion of the fields requires a solution of a sparse matrix equation and its cost is negligible. However, the sparse matrix involves discretized identity operators, which may deteriorate the accuracy of the results. An alternative and accurate way to expand the incident fields is to solve the discrete form of the equation [17]

$$\hat{\boldsymbol{t}} \cdot \begin{bmatrix} \eta_1\mathcal{T}_1 & -\mathcal{K}_1 \\ \mathcal{K}_1 & \eta_1^{-1}\mathcal{T}_1 \end{bmatrix} \cdot \begin{bmatrix} \boldsymbol{J}^{inc}(\boldsymbol{r}) \\ \boldsymbol{M}^{inc}(\boldsymbol{r}) \end{bmatrix} = -\frac{1}{2}\hat{\boldsymbol{t}} \cdot \begin{bmatrix} \boldsymbol{E}^{inc}(\boldsymbol{r}) \\ \boldsymbol{H}^{inc}(\boldsymbol{r}) \end{bmatrix}, \qquad (44)$$

which is completely free of the identity operator. Then, the stabilization of CTF involves the solution of a dense matrix equation in addition to the solution of the original equation. The resulting stable formulation is called double-stabilized CTF (DS-CTF) [17].

Although S-CTF and DS-CTF provide accurate results for

low-contrast problems that cannot be solved accurately with the conventional formulations, they also have limitations; they break down when the contrast is decreased to very low values. For accurate solutions of arbitrarily low-contrast problems, we propose the field-based-stabilized CTF (FBS-CTF) [17], derived as

$$\begin{aligned}\hat{\boldsymbol{t}}\cdot\begin{bmatrix}\eta_1\mathcal{T}_1+\eta_2\mathcal{T}_2 & -\Big(\mathcal{K}_1+\mathcal{K}_2\Big)\\ \eta_1\eta_2\Big(\mathcal{K}_1+\mathcal{K}_2\Big) & \eta_2\mathcal{T}_1+\eta_1\mathcal{T}_2\end{bmatrix}\cdot\begin{bmatrix}\boldsymbol{J}^r(\boldsymbol{r})\\ \boldsymbol{M}^r(\boldsymbol{r})\end{bmatrix}\\ =-\frac{1}{2}\hat{\boldsymbol{t}}\cdot\begin{bmatrix}\boldsymbol{E}^{inc}(\boldsymbol{r})-\boldsymbol{E}_2^{inc}(\boldsymbol{r})\\ \eta_2\eta_1\boldsymbol{H}^{inc}(\boldsymbol{r})-\eta_2\eta_1\boldsymbol{H}_2^{inc}(\boldsymbol{r})\end{bmatrix}\\ -\hat{\boldsymbol{t}}\cdot\begin{bmatrix}\eta_2\mathcal{T}_2 & -\mathcal{K}_2\\ \eta_1\eta_2\mathcal{K}_2 & \eta_1\mathcal{T}_2\end{bmatrix}\cdot\begin{bmatrix}\boldsymbol{J}^{inc}(\boldsymbol{r})-\hat{\boldsymbol{n}}\times\boldsymbol{H}_2^{inc}(\boldsymbol{r})\\ \boldsymbol{M}^{inc}(\boldsymbol{r})+\hat{\boldsymbol{n}}\times\boldsymbol{E}_2^{inc}(\boldsymbol{r})\end{bmatrix}.\end{aligned} \tag{45}$$

In the above, $\boldsymbol{E}_2^{inc}(\boldsymbol{r})$ and $\boldsymbol{H}_2^{inc}(\boldsymbol{r})$ are fictitious incident fields defined as

$$\{\boldsymbol{E}_2^{inc}(\boldsymbol{r}),\boldsymbol{H}_2^{inc}(\boldsymbol{r})\}=\lim_{\substack{\epsilon_2\to\epsilon_1\\ \mu_2\to\mu_1}}\{\boldsymbol{E}^{inc}(\boldsymbol{r}),\boldsymbol{H}^{inc}(\boldsymbol{r})\}. \tag{46}$$

We note that LHS of FBS-CTF is the same as the LHS of CTF; it requires a modification only on the RHS of the conventional formulation, similar to S-CTF and DS-CTF.

Fig. 4 presents the results of scattering problems involving a sphere of radius 6λ discretized with 264,006 RWG functions. Scattering problems are solved by 5-level MLFMA, where the near-field and far-field interactions are calculated with 1% error. The sphere is in free space, it has various relative permittivities from $\epsilon_r=1+10^{-1}$ to $\epsilon_r=1+10^{-9}$, and it is illuminated by a plane wave propagating in the z direction with the electric field polarized in the x direction. Fig. 4(a) presents the relative root-mean-square (RMS) error as a function of the contrast (ϵ_r-1). To calculate the error, we first compute the far-zone electric field on the $\phi=0^\circ$ plane at $p=360$ points from 0° to 180°. Then, the relative RMS error is defined as

$$e_{RMS}=\frac{||\boldsymbol{E}_C-\boldsymbol{E}_A||_2}{||\boldsymbol{E}_A||_2}, \tag{47}$$

where $\boldsymbol{E}_C$ and $\boldsymbol{E}_A$ are the computational and analytical values (arrays of p elements containing co-polar electric fields), respectively, and $||.||_2$ represents the 2-norm of the arrays. Fig. 4(a) shows that the RMS error of CTF increases sharply when the contrast decreases below 10^{-1}, while S-CTF and DS-CTF break down when the contrast is about 10^{-5}. On the other hand, the error of FBS-CTF is almost constant with respect to the contrast. We also note the relatively high accuracy of DS-CTF, which is completely free of the identity operator, in the $10^{-1}-10^{-5}$ range. Finally, Fig. 4(b) depicts the bistatic RCS values on the $\phi=0^\circ$ plane when the contrast of the sphere is 10^{-6}. We observe that all formulations, except for the FBS-CTF, fail to provide accurate results compared to Mie-series solution.

VI. Conclusion

In this paper, we consider accurate and efficient solutions of scattering problems involving large dielectric objects with moderate and low contrasts. When the problem size is large, JMCFIE accelerated with a block preconditioner is preferable for efficient solutions. We report various procedures to stabilize the surface formulations for accurate solutions of low-contrast dielectric problems.

Acknowledgment

This work was supported by the Scientific and Technical Research Council of Turkey (TUBITAK) under Research Grant 105E172, by the Turkish Academy of Sciences in the framework of the Young Scientist Award Program (LG/TUBA-GEBIP/2002-1-12), and by contracts from ASELSAN and SSM.

References

[1] A. J. Poggio and E. K. Miller, "Integral equation solutions of three-dimensional scattering problems," in *Computer Techniques for Electromagnetics*, R. Mittra, Ed. Oxford: Pergamon Press, 1973, Chap. 4.

[2] C. Müller, *Foundations of the Mathematical Theory of Electromagnetic Waves*. New York: Springer, 1969.

[3] X.-Q. Sheng, J.-M. Jin, J. Song, W. C. Chew, and C.-C. Lu, "Solution of combined-field integral equation using multilevel fast multipole algorithm for scattering by homogeneous bodies," *IEEE Trans. Antennas Propagat.*, vol. 46, no. 11, pp. 1718–1726, Nov. 1998.

[4] P. Ylä-Oijala and M. Taskinen, "Well-conditioned Müller formulation for electromagnetic scattering by dielectric objects," *IEEE Trans. Antennas Propagat.*, vol. 53, no. 10, pp. 3316–3323, Oct. 2005.

[5] P. Ylä-Oijala, M. Taskinen, and S. Järvenpää, "Surface integral equation formulations for solving electromagnetic scattering problems with iterative methods," *Radio Science*, vol. 40, RS6002, Nov. 2005.

[6] P. Ylä-Oijala and M. Taskinen, "Application of combined field integral equation for electromagnetic scattering by dielectric and composite objects," *IEEE Trans. Antennas Propagat.*, vol. 53, no. 3, pp. 1168–1173, Mar. 2005.

[7] J. Song, C.-C. Lu, and W. C. Chew, "Multilevel fast multipole algorithm for electromagnetic scattering by large complex objects," *IEEE Trans. Antennas Propagat.*, vol. 45, no. 10, pp. 1488–1493, Oct. 1997.

[8] L. Gürel and Ö. Ergül, "Comparisons of FMM implementations employing different formulations and iterative solvers," in *Proc. IEEE Antennas and Propagation Soc. Int. Symp.*, vol. 1, 2003, pp. 19–22.

[9] Ö. Ergül and L. Gürel, "Investigation of the inaccuracy of the MFIE discretized with the RWG basis functions," in *Proc. IEEE Antennas and Propagation Soc. Int. Symp.*, vol. 3, 2004, pp. 3393–3396.

[10] L. Gürel and W. C. Chew, "Recursive algorithms for calculating the scattering from N strips or patches," *IEEE Trans. Antennas Propagat.*, vol. AP-38, pp. 507–515, Apr. 1990.

[11] D. A. Hill, "Electromagnetic scattering by buried objects of low contrast," *IEEE Trans. Geosci. Remote Sen.*, vol. 26, no. 2, pp. 195–203, Mar. 1988.

[12] E. S. Thiele, "Scattering of electromagnetic radiation by complex microstructures in the resonant regime," Ph.D. thesis, University of Pennsylvania, 1998.

[13] T. W. Lloyd, J. M. Song, and M. Yang, "Numerical study of surface integral formulations for low-contrast objects," *IEEE Antennas Wireless Propagat. Lett.*, vol. 4, pp. 482–485, 2005.

[14] P. Loschialpo, D. W. Forester, and J. Schelleng, "Anomalous transmission through near unit index contrast dielectric photonic crystals," *J. Appl. Phys.*, vol. 86, no. 10, pp. 5342–5347, Nov. 1999.

[15] P. M. Goggans and A. Glisson, "A surface integral equation formulation for low contrast scatterers based on radiation currents," *ACES Journal*, vol. 10, pp. 15–18, Mar. 1995.

[16] Ö. Ergül and L. Gürel, "Improving the accuracy of the surface integral equations for low-contrast dielectric scatterers," *2007 IEEE International Symposium on Antennas and Propagation*, Honolulu, Hawai'i, USA, June 2007.

[17] Ö. Ergül and L. Gürel, "Stabilization of integral-equation formulations for accurate solution of scattering problems involving low-contrast dielectric objects," *IEEE Trans. Antennas Propagat.*, submitted for publication.